Available online at www.sciencedirect.com

ScienceDirect

Procedia Structural Integrity 7 (2017) 149–157

Structural Integrity Procedia

www.elsevier.com/locate/procedia

3rd International Symposium on Fatigue Design and Material Defects, FDMD 2017, 19-22 September 2017, Lecco, Italy

Influence of build orientation on static and axial fatigue properties of maraging steel specimens produced by additive manufacturing

G. Meneghetti[a,*]*, D. Rigon[a], D. Cozzi[b], W. Waldhauser[b], M. Dabalà[a]

[a]*Department of Industrial Engineering, University of Padova, via Venezia, 1 – 35131 Padova (Italy)*
[b]*Joanneum Research Forschungsgesellschaft mbH, Institute for Surface Technologies and Photonics, Niklasdorf Leobner Straße, 94 A-8712 Niklasdorf, (Austria)*

Abstract

Additive manufacturing involves a layer-by-layer build-up of mechanical parts and it is a manufacturing technology that can be adopted with different engineering metal materials like steels, aluminium and titanium alloys. Aim of the present investigation is to analyse the influence of the build orientation on static and axial fatigue properties of maraging steel specimens manufactured by Direct Metal Laser Sintering (DMLS) of EOS metal powders. After manufacturing, some of the specimens were subjected to age hardening heat treatment (490 °C for 6 hours, followed by air cooling). Both heat treated and as-manufactured specimens have been built at 0° as well as at 90° orientation with respect to the specimen's axis. Analyses of the crack initiation point are performed in order to investigate the fatigue failure mechanisms. Finally, the fatigue strength of the additively manufactured specimens was compared with that exhibited by vacuum melted specimens of the same steel reported in literature.

Peer-review under responsibility of the Scientific Committee of the 3rd International Symposium on Fatigue Design and Material Defects.

Keywords: Additive manufacturing; Maraging steel; Axial fatigue

* Corresponding author. Tel.: +39-0498276751.
E-mail address: giovanni.meneghetti@unipd.it

Peer-review under responsibility of the Scientific Committee of the 3rd International Symposium on Fatigue Design and Material Defects.
10.1016/j.prostr.2017.11.072

1. Introduction

Additive manufacturing (AM) techniques have been known for more than 20 years and were at first applied to rapid manufacture prototypes, where porosity was not an issue (Beaman and Deckard, (1990)). In the last 10 years AM of parts increased thanks to the advancement of technology, which led to improved part density and quality with the enormous advantage of design freedom (Kruth et al. (2005); Rannar et al., (2007); Murr et al., (2012); Kranz et al., (2015)).

Nomenclature

DMLS	direct metal laser sintering
Δf	specimen deflection
NT	not aging hardening heat-treated specimens
T	aging hardening heat-treated specimens
R_a	surface roughness
ε_m	mean strain
ε_R	elongation at fracture
σ_a	cyclic stress amplitude
σ_R	ultimate tensile strength

AM of metals can be presently performed by using different methods: Laser Beam Melting (LBM), Electron Beam Melting (EBM) and Laser Metal Deposition (LMD) (also known as Direct Energy Deposition (DED)) (Yan and Yu, (2015)). Irrespective of the adopted technology, the starting point of metal AM processes is a 3D CAD model, which is sliced in the computer virtual environment into thin layers (the layer thickness being in the range 20 micrometers – 1 mm). Afterwards, the physical component is built by layer-by-layer deposition and locally melting of the material using a heat source (the laser beam or the electron beam) depending on the AM process.

All AM processes involve complex thermal cycles, where cooling rates are reported to be extremely high, i.e. on the order of 10^3–10^8 K/s in LBM processes (Gu et al., (2012)). Since heat conduction is likely to be more effective in the building direction than in the transversal direction, elongated grain shapes have been observed leading to anisotropy of microstructure and of resulting mechanical properties.

The adopted process of AM of metals and the post-manufacturing heat and surface treatment result in final static and fatigue properties of the part. With the advancement in the AM technology dense part can now be achieved as compared to conventional manufacturing processes (cast or wrought parts). It is reported that high density is the first goal in AM process optimization in order to reduce pore formation (Everton et al., (2016)), which is detrimental in static and, to a larger extent, in fatigue strength. Generally speaking, microstructure of AM parts is finer than that obtained by means of traditional processes (e.g. casting): therefore, static mechanical properties (yield and tensile strengths) are often higher, while maintaining approximately the same ductility. This result can be found for example by comparing the static properties of wrought (ASTM A276) and additively manufactured (by LMD) 316L stainless steel (Carlton et al., (2016) and Wang et al., (2016)), of cast (EN 1706) and LBM AlSi10Mg aluminium alloy (Manfredi et al., (2014), of wrought (Donachie, (2000)) and LBM Ti-6Al-4V titanium alloy (Xu et al., (2015)).

Similarly to the static mechanical properties, structural durability is of major concern in design structural components. Therefore, a number of fatigue studies have been reported in the literature. As a general remark, microstructure, surface roughness and size/distribution of material defects strongly influence the fatigue strength. Generally speaking, additive manufacturing does not produce final parts because different degrees of post processing are required to achieve the target properties. Reduction of remaining porosity, mitigation of inner residual stresses, preparation of functional surfaces is often achieved by means of hot isostatic pressure (HIP), heat treatment, machining/micro-machining, surface treatments like sand blasting or micro-shot peening. Less fatigue studies are reported in the literature as compared to static strength studies (see for example the recent extensive review on additive manufacturing of metals by (Herzog et al., (2016)).

Leuders et al. (2013) studied the fatigue crack propagation resistance of as-built, heat treated and HIPed SLM-processed Ti-6Al-4V titanium alloy and reported that microstructure, pore size and internal residual stresses have a fundamental role in determining the resulting fatigue properties. Fracture mechanics-based studies of the anisotropic behaviour of SLM-processed metals have been performed recently (Konečná et al., (2016) and (2017)); defect sensitivity has also been compared between additively manufactured and traditionally manufactured metals (Beretta and Romano, (2017)). Mower and Long (2015) compared the static strength and fatigue behavior of additively manufactured AlSi10Mg, Ti-6Al-4V, and two stainless steel (316L and 17-4PH) with the same alloys produced by traditional methods (wrought and machined). Nicoletto (2017) analysed the HCF behaviour of Ti-6Al-4V titanium alloy in plane bending fatigue, while Li et al. (2016) highlighted the key role of surface roughness in fatigue performances of Ti-6Al-4V AM specimens.

Concerning maraging steels, which is a high-strength material adopted in aeronautical and tool fields and which the present contribution is focused on, Kempen et al., (2011) report the influence of the laser speed, the layers thickness and the post-aging treatment on the hardness and static properties of maraging steel grade 300 additively manufactured (by Selective Laser Melted (SLM)) comparing them to those obtained from wrought material. Croccolo et al., (2016), inspired by the contributions on titanium alloy of Edwards and Ramulu, (2014) and (2015), studied the influence of the building orientation on the high cycle rotating bending fatigue life of the EOS maraging steel produced by a EOS additive manufacturing machine.

According to the authors knowledge, there is a lack of data in the literature concerning axial fatigue strength of additively manufactured maraging steel. Therefore, this contribution analyses the influence of the building direction and the age hardening treatment on static and axial fatigue behavior of EOS maraging steel MS1 realized by Direct Metal Laser Sintering (DMLS); afterwards, the results are compared with those of vacuum melted maraging steel 300 specimens as reported in literature (Van Swam et al., (1973)).

In AM Powder bed Fusion technologies, the solidification of subsequent layers of material and the large thermal gradient involved induce tensile residual stresses that are detrimental in fatigue performances (Mercelis P., Kruth J., (2006)). Furthermore, due to residual stresses geometrical tolerances might be lost after detaching the specimens from the building platform. As a consequence, in axial fatigue tests the resulting geometrical distortion induces secondary bending, i.e. mean stress effects. For this reason, the mean stress was analysed by correlating the specimens' eccentricity and the mean strain measured by means of strain gauges. Finally, fracture surfaces of some specimens have been observed by means of stereoscopic microscope in order to identify the cause of the fatigue damage.

2. Materials and methods

Tensile static tests and fully reversed (R = -1), load-controlled axial fatigue tests were carried out on cylindrical specimens additively manufactured by DMLS by adopting EOS maraging steel MS1 powder, whose chemical composition is reported in Table 1. The adopted specimen's geometry is shown in Fig.1a. Specimens have been manufactured by using a EOSINT M280, having a building volume of 250 mm x 250 mm x 350 mm and being equipped with ytterbium fibre laser with a wavelength of 1064 nm, a variable focus diameter ranging from 100 and 500 μm and a laser scan speed that could be set up to 7 m/s.

The specimen building direction has been set at an orientation of 0° and of 90° with respect to the specimen's longitudinal axis (see Fig.1b), by setting a layer thickness equals to 40 μm, a laser power of 400 W and by adopting as set of parameters the so-called "Performance 1.0" as optimized by EOS GmbH with the aim of obtaining the best compromise between the manufacturing time and the resulting mechanical properties. It should be noted that the set of parameters "Performance 1.0" is given as an implemented tool, so that setting the value of a single parameter is not allowed. After manufacturing, half of the specimens, i.e. 24 specimens, have been subjected to age hardening heat treatment at 490 °C for 6 hours, followed by air cooling as recommended by the powder manufacturer, while the remaining half of them has been kept in as-built conditions.

Table 1. Chemical composition of EOS maraging steel MS1 powder from technical EOS datasheet.

Fe (wt-%)	Ni (wt-%)	Co (wt-%)	Mo (wt-%)	Ti (wt-%)	Al (wt-%)	Cr (wt-%)	Cu (wt-%)	C (wt-%)	Mn (wt-%)	Si (wt-%)	P (wt-%)	S (wt-%)
balance	17-19	8.5-9.5	4.5-5.2	0.6-0.8	0.05-0.15	≤ 0.5	≤ 0.5	≤ 0.03	≤ 0.1	≤ 0.1	≤ 0.01	≤ 0.01

The specimens have been detached from the building platform by using a liquid-cooled band saw and, then, the lattice supports have been removed by using an abrasive grinding wheel. Afterwards, the specimens surface has been accurately polished by using progressively finer sandpapers, from grade 100 up to grade 800.

a) b)

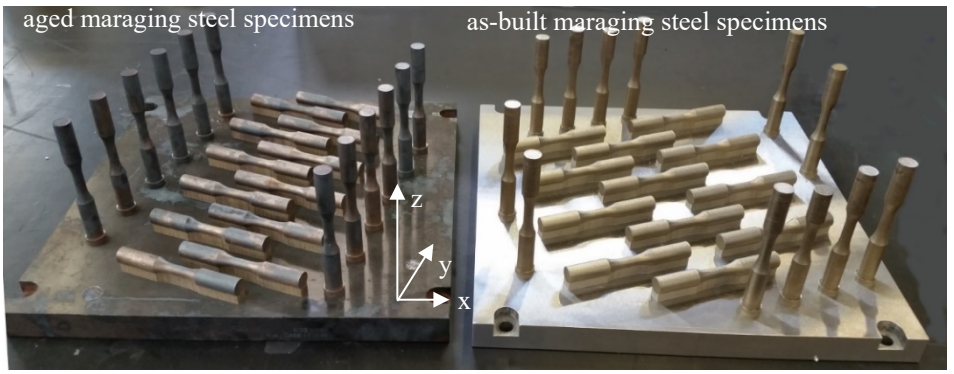

Fig. 1. (a) Specimen's geometry adopted for tensile static and fatigue tests on maraging steel produced by DMLS, and (b) two building platforms with the specimens produced by DMLS having specimen's axis oriented at 0° and 90° with respect to the building direction (z axis).

The static and fatigue tests were carried out by using a servo-hydraulic SCHENCK HYDROPULS PSA 100 machine having a 100 kN load cell and equipped with a TRIO Sistemi RT3 digital controller. Tensile static tests with a displacement rate equal to 2 mm/min have been carried out by adopting the uniaxial MTS extensometer having gauge length of 5 mm. Concerning the load-controlled fatigue tests, the load frequency has been set in the range between 10 Hz and 30 Hz, depending on the applied load level.

When detaching the specimens from the building platform, the residual stresses due to the previous DMLS process could generate a certain level of bending distortion of the specimens. Therefore, the resulting deflection Δf (see Fig. 2a) was measured by clamping one side of each specimen and by using a digital dial gauge in contact with the opposite side of the specimen. Bending distortion causes a secondary bending when specimens are clamped in the axial test machine grips, thus resulting in a mean axial strain, which has been measured by using KYOWA strain gauges having a gauge length of 3 mm. Strain measurements have been performed only for selected specimens having different values of deflection Δf, so that the relation between Δf and the mean strain could be determined. The strain gauges have been applied at the middle of the specimen at locations A and B, as shown in Fig. 2a. A picture of a specimen with strain gauge located at the point A is shown in Fig. 2b.

In the following, each test series will be identified according to the nomenclature *AD_0°/90°_NT/T_specimen's number*, where *AD* represents the additively manufactured series, 0° and 90° are the orientation of the building directions with respect to the specimen's longitudinal axis, while *NT* and *T* identify the series tested in the as-built and in the heat-treated conditions, respectively.

a)

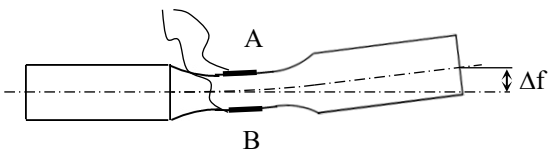

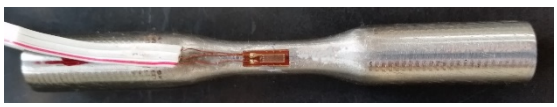

Fig. 2. (a) Location of strain gauges adopted to evaluate the correlation between deflection Δf and mean axial strain induced by clamping in the axial machine grips and (b) example of specimen with a strain gauge placed at point A.

3. Roughness and geometrical distortions measurements

The roughness parameter R_a has been measured along the specimens' axis for 5 samples of each test series by using a surface roughness tester (Taylor Hobson precision – Surtronic 25) having a resolution of 0.01 μm. The range of R_a values as obtained for each test series is reported in Table 2 along with the range of the deflection values Δf caused by residual stresses induced by DMLS. It should be noted that the deflection values Δf obtained from heat-treated specimens (T) are lower than those obtained from as-built specimens, since residual stresses induced by DMLS process are likely to be relieved by the aging treatment.

Table 2. Roughness and deflection range values.

Series identifier	R_a * [μm]	Δf ° [mm]
AD_0°_NT_#	0.45-0.77	0.22-1.03
AD_0°_T_#	0.53-0.52	0.11-0.25
AD_90°_NT_#	0.36-0.56	0.58-0.98
AD_90°_T_#	0.25-0.57	0.27-0.57

* Measurements carried out for 5 specimens per series

° Measurements carried out for all specimens

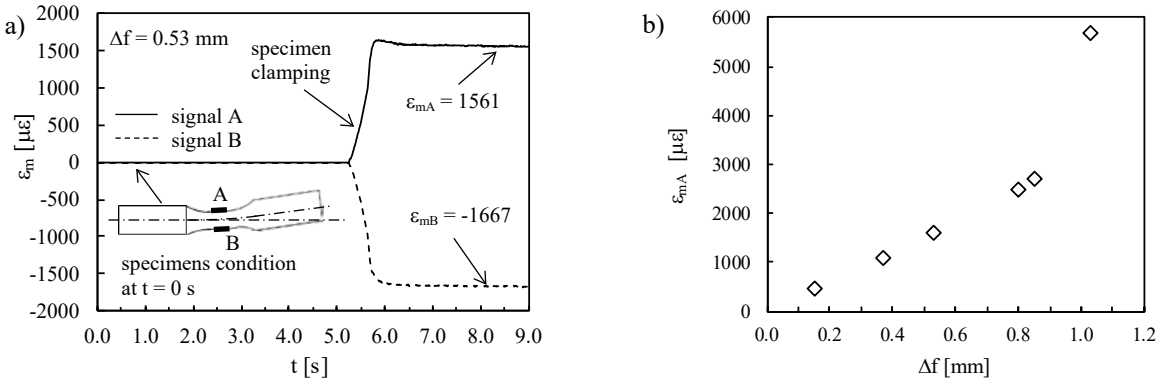

Fig. 3. (a) An example of strain measurement at the midpoint of the inner side of the specimen curvature (point A) and at the opposite side (point B) during the specimen clamping on the test machine and (b) correlation between mean strain measurements at point A and deflection Δf for selected specimens.

Fig. 3a reports the strain measurements at points A and B referred to a specimen with Δf = 0.53 mm before and after clamping. As expected, after clamping plane bending is induced, being ε_m almost equal in modulus but with opposite sign at points A and B. Fig. 3b reports the correlation between the axial strain ε_{mA} as measured at point A and the bending deflection Δf for selected specimens.

4. Tensile test results

A tensile stress-strain curve obtained from the static test of one specimen for each test series is reported in Fig. 4a. The starting point of the dashed lines is the point when the extensometer was removed, as its full scale having been achieved. The mechanical properties obtained from the tensile tests are reported in Fig. 4b for each test series. As a result, the Young's modulus E, the yield strength $\sigma_{p,02}$ and the ultimate tensile strength σ_R are in good

agreement with those reported in (Kempen et al. (2011)). Fig. 4b also reports the values of elongation after fracture ε_R, which are higher than those reported in Kempen et al. (2011).

5. Fatigue test results

The experimental results obtained from fully reversed (R=-1) load-controlled fatigue tests, are presented in Fig. 5a for the four tests series in terms of nominal stress amplitude. In order to take into account the different mean stresses caused by specimens' distortion illustrated previously, the SWT parameter was evaluated for each specimens at the crack initiation point (Fig 5b) (Smith et al., (1970)).

a)

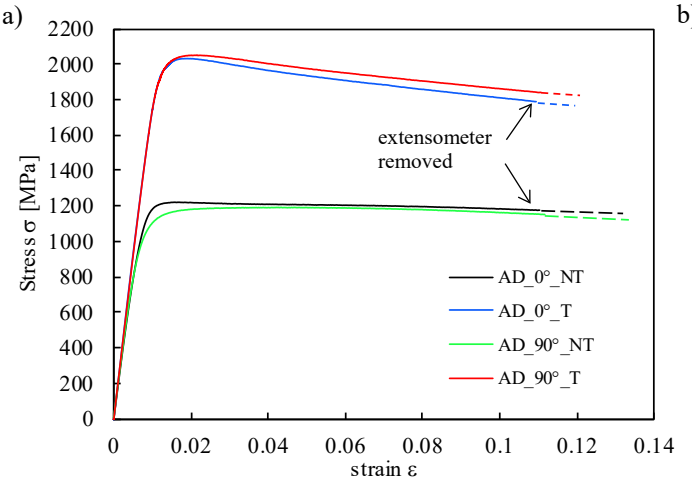

b)

Spec. code	E [MPa]	σ_R [MPa]	$\sigma_{p0,2}$ [MPa]	ε_R [%]
AD_0°_NT_7	169050	1213	1120	33.6%
AD_0°_NT_8	168790	1220	1130	36.2%
AD_0°_T_2	187010	2029	1950	10.3%
AD_0°_T_11	189020	2038	1970	9.30%
AD_90°_NT_1	170620	1215	1030	29.1%
AD_90°_NT_4	169980	1190	1035	29.7%
AD_90°_T_4	187460	2055	1950	14.3%

Fig. 4. (a) Stress-strain curves of the DMLS specimens tested in the as-built (not-treated NT) and aged (treated T) conditions with different building orientation (0° and 90°) and (b) summary of mechanical properties.

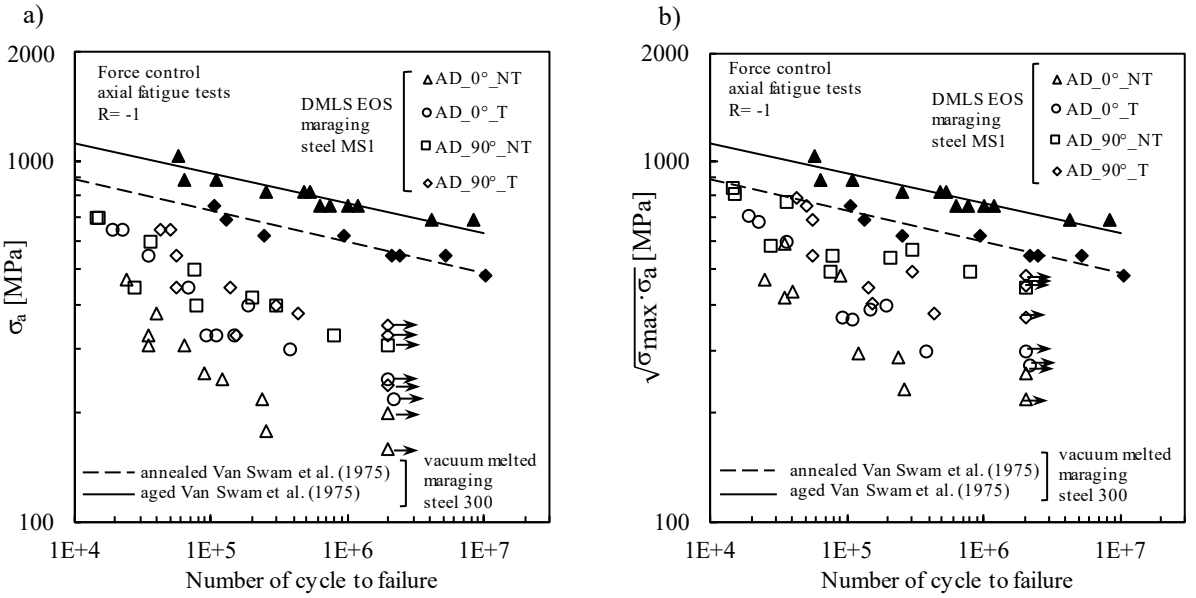

Fig. 5. (a) Fatigue test results in terms of nominal stress amplitude for the DMLS specimens tested in the as-built (not-treated NT) and aged (heat treated T) conditions with different building orientations (0° and 90°). Comparison with fatigue test results obtained by Van Swam et al. (1975) by testing vacuum melted maraging steel 300 under push-pull axial loading. (b) Fatigue test results in terms of SWT parameter, evaluated individually at the crack initiation point of the specimens.

For comparison purposes, Fig. 5a and b reports also push-pull axial fatigue data relevant to vacuum melted maraging steel 300 in dry argon environment (Van Swam et al. (1975)), tested under both annealed (1 h at 820 °C air cooled) or annealed followed by aged condition (3 h at 480 °C air cooled). In Fig. 5b it is worth noting that the AM fatigue test results are closer to the results of the vacuum melted maraging steel with respect to those in terms of nominal amplitude stress, but the scatters of the single series are not decreased. However, it should be noted that some DMLS specimens show a premature fatigue failure as compared to the trend shown by the other tested specimens belonging to the same test series. An inspection of the fracture surfaces has been carried out by means of stereoscopic microscope in order to investigate these particular cases. For example, analyzing the fracture surfaces of two specimens of the series AD_90°_NT subjected to the same amplitude stress level and having approximately the same Δf (i.e. the same superimposed mean stress), one of them underwent premature failure due to a surface defect relatively larger than the one found in the other one (see Fig 6a and Fig. 6b). Consequently, the local evaluated SWT parameter is not able to reduce the scatter of the fatigue test results. A unified treatment of the fatigue limit of materials having defects, blunt and severe notches has been proposed in the past in Atzori et al., (2003), Atzori et al., (2005) and Meneghetti and Masaggia (2012).

Despite the large scatter of the AM results, it can be observed that the test series referred to 0° building direction exhibit a lower fatigue strength than those referred to 90° orientation, both for as-built and aged conditions. Furthermore, it is worth noting that the age hardening treatment improved the fatigue strength for the series having 0° building direction. Conversely, for the specimens built at 90° orientation, the aging heat treatment did not lead to significant fatigue strength improvement. The fatigue strength of all additively manufactured test series is lower than the vacuum melted maraging steel 300.

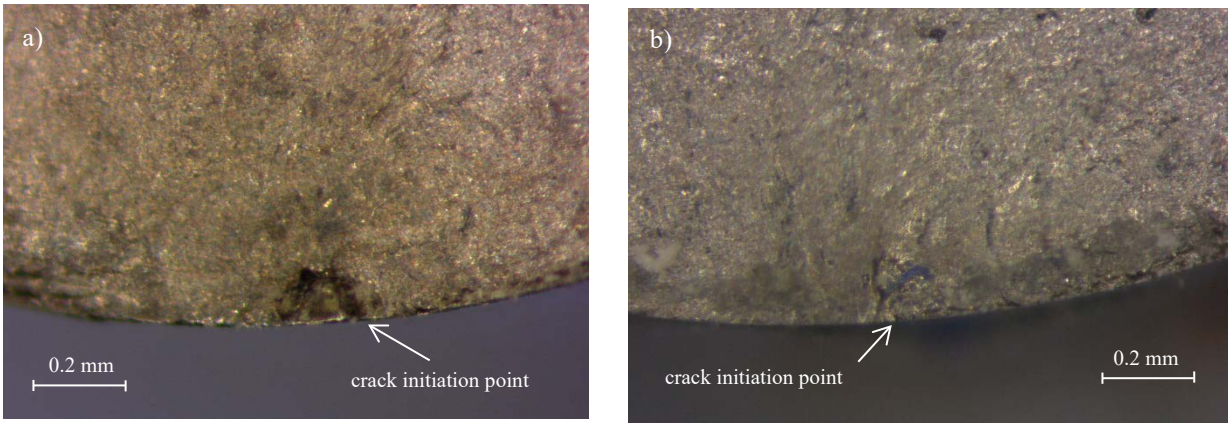

Fig. 6. Crack initiation point analysed by means of a stereoscopic microscope for: (a) AD_90°_NT specimen subjected to $\sigma_a = 400$ MPa, having $\Delta f = 0.73$ mm, and failed at $7.75 \cdot 10^4$ cycles, and (b) AD_90°_NT specimen subjected to $\sigma_a = 400$ MPa, having $\Delta f = 0.85$ mm, and failed at $2.99 \cdot 10^5$ cycles.

6. Conclusions

The influence of building direction (at 0° and 90° with respect to the specimen's longitudinal axis, respectively) and of age hardening heat treatment on static and fatigue properties of additively manufactured maraging steel 300 MS1 specimens has been investigated. The results of static tensile tests indicated that there is no difference in terms of mechanical properties between 0° and 90° specimen building-orientation, both for as-built and aged conditions; this result is in agreement with the relevant literature. However, in the present contribution the elongation after fracture has been found higher than that reported in the literature. The effect of the mean stress caused by the distortion of the specimens due the residual stresses induces by the AM process was taken into account by means of the SWT parameter evaluated at the crack initiation point. However, the scatter does not reduce because of the presence of surface defects having different sizes. In spite of the large scatter of the test series, the axial fatigue results indicated that the lowest fatigue strength occurs for 0°- oriented specimens. Regarding the heat treatment, the fatigue strength of as-built (NT), 0° oriented specimens was found slightly lower than heat treated (T) specimens having the same building orientation, whereas for the 90° oriented specimens the scatter of the results did not allow

to single out significant differences between the (NT) and (T) series. For comparison purposes, all experimental results have also been compared with data taken from the literature and obtained by fatigue testing vacuum melted maraging steel 300 under both annealed and annealed followed by age hardened conditions. By taking the fatigue strengths at $5.0 \cdot 10^5$ cycles as reference values, the test series AD_0°_NT and AD_90°_NT show 72% and 33% lower fatigue strength with respect to that of vacuum melted maraging in annealed condition, respectively. The test series AD_0°_T and AD_90°_T show 68% and 61% lower fatigue strengths as compared to that of vacuum melted maraging steel in annealed followed by age hardened conditions.

References

ASTM A276, Standard Specification for Stainless Steel Bars and Shapes.

Atzori, B., Lazzarin, P., Meneghetti, G., 2003. Fracture Mechanics and Notch Sensitivity, Fatigue & Fracture of Engineering Materials and Structures, 26 (3), 257-267.

Atzori, B., Lazzarin, P., Meneghetti, G., 2005. A unified treatment of the mode I fatigue limit of components containing notches or defects, International Journal of Fracture, 133 (1), 61–87.

Beaman, J. J., Deckard, C. R., 1990. Selective laser sintering with assisted powder handling, US patent no. 4938816.

Beretta, S., Romano, S., 2017. A comparison of fatigue strength sensitivity to defects for materials manufactured by AM or traditional processes, International Journal of Fatigue, 94, 178-191.

Carlton, H. D., Haboub, A., Gallegos, G.F., Parkinson, D.Y., 2016. Damage evolution and failure mechanisms in additively manufactured stainless steel, Materials Science and Engineering: A, 651, 406-414.

Croccolo, D., De Agostinis, M., Fini, S., Olmi, G., Vranic, A., Ciric-Kostic, S., 2016. Influence of the build orientation on the fatigue strength of EOS maraging steel produced by additive metal machine, Fatigue & Fracture of Engineering Materials and Structures, 39, 151-158.

Donachie, M.J. Titanium: a Technical Guide, second ed., ASM International, Materials Park, 2000.

DIN EN 1706, Aluminium and Aluminium Alloys - Castings - Chemical Composition and Mechanical Properties, 2013-12.

Edwards, P., Ramulu, M., 2014. Fatigue performance evalu- ation of selective laser melted Ti-6Al-4V. Materials Science and Engineering A, 598, 327-337.

Edwards, P., Ramulu, M., 2015. Effect of build direction on the fracture toughness and fatigue crack growth in selective laser melted Ti-6Al-4V. Fatigue & Fracture of Engineering Materials and Structures, 38 (10), 1228-1236.

Everton, S.K., Hirsch, M., Stravroulakis, P., Leach, R.K., Clare, A.T., 2016. Review of in-situ process monitoring and in-situ metrology for metal additive manufacturing. Materials & Design, 95, 431-445.

Gu, D., Hagedorn, Y., Meiners, W., Meng, G., Santos Batista, R.J., Wissenbach, K., Poprawe, R., 2012. Densification behavior, microstructure evolution, and wear performance of selective laser melting processed commercially pure titanium. Acta Materialia, 60 (9), 3849-3860.

Herzog, D., Seyda, V., Wycisk, E., Emmelmann, C., 2016. Additive manufacturing of metals, Acta Materialia, 117, 371-392.

Kempen, K., Yasa, E., Thijs, L., Kruth, J.P., Van Humbeeck, J., 2011. Microstructure and mechanical properties of Selective Laser Melted 18Ni-300 steel, Physics Procedia, 12, 255-263.

Konečná, R., Kunz, L., Bača, A., Nicoletto, G., 2017. Resistance of direct metal laser sintered Ti6Al4V alloy against growth of fatigue cracks, Engineering Fracture Mechanics, in press.

Konečná, R., Kunz, L., Nicoletto, G., Bača, A., 2016. Long fatigue crack growth in Inconel 718 produced by selective laser melting, International Journal of Fatigue, 92, 499-506.

Kranz, J., Herzog, D., Emmelmann, C., 2015. Design guidelines for laser additive manufacturing of lightweight structures in TiAl6V4, Journal of Laser Applications, 27.

Kruth, J. P., Vandenbroucke, B., van Vaerenbergh, J., Naert, I., 2005. Rapid manufacturing of dental prostheses by means of selective laser sintering/ melting, Proc AFPR, S4.

Leuders, S, Thöne, M., Riemer, A., Niendorf, T., Tröster, T., Richard, H.A., Maier, H.J., 2013. On the mechanical behaviour of titanium alloy TiAl6V4 manufactured by selective laser melting: fatigue resistance and crack growth performance, International Journal of Fatigue, 48, 300-307.

Li, P., Warner, D.H., Fatemi, A., Phan, N., 2016. Critical assessment of the fatigue performance of additively manufactured Ti–6Al–4V and perspective for future research, International Journal of Fatigue, 85, 130-143.

Manfredi, D., Calignano, F., Krishnan, M., Canali, R., Ambrosio, E.P., Biamino, S., Ugues, D., Pavese, M., Fino, P., 2014. Additive manufacturing of Al alloys and aluminium matrix composites (AMCs), Light Metal Alloys Applications.

Meneghetti, G., Masaggia, S., 2012 Estimation of the fatigue limit of components made of Austempered Ductile Iron weakened by V-shaped notches, Proceedings of the 70th World Foundry Congress WFC 2012, Monterrey, Mexico.

Mercelis P., Kruth J., (2006). Residual stresses in selective laser sintering and selective laser melting. Rapid Prototyping Journal, 12 (5), 254-265.

Mower, T.M., Long, M.J., 2016. Mechanical behavior of additive manufactured, powder-bed laser-fused materials, Materials Science and Engineering A, 651, 193-213.

Murr, L.E., Gaytan, S.M., Ramirez, D.A., Martinez, E., Hernandez, J., Amato, K.N., Shindo, P.W., Medina, F.R., Wicker, R.B., 2012. Metal fabrication by additive manufacturing using laser and electron beam melting technologies, Journal of Materials Science & Technology, 28 (1), 1-14.

Nicoletto, G., 2017. Anisotropic high cycle fatigue behavior of Ti–6Al–4V obtained by powder bed laser fusion, International Journal of Fatigue, 94, 255-262.

Rannar, L.E., Glad, A., Gustafson, C.G., 2007. Efficient cooling with tool inserts manufactured by electron beam melting, Rapid Prototyping Journal, 13 (3), 128-135.

Smith, K. N., Watson, P., Topper, T. H., 1970. A Stress-Strain Function for the Fatigue of Metals, Journal of Materials, ASTM, vol. 5, no. 4, Dec. 1970.

Xu, W., Brandt, M., Sun, S., Elambasseril, J., Liu, Q., Latham, K., Xia, K., Qian, M., 2015. Additive manufacturing of strong and ductile Ti-6Al-4V by selective laser melting via in situ martensite decomposition, Acta Materialia, 85, 74-84.

Van Swam, LF, Pelloux, RM, Grant, NJ, 1975. Fatigue behavior of maraging steel 300. Metallurgical Transactions A, 6 (1), 45-54.

Wang, Z., Palmer, T.A., Beese, A.M., 2015. Effect of processing parameters on microstructure and tensile properties of austenitic stainless steel 304L made by directed energy deposition additive manufacturing, Acta Materialia, 110, 226-235.

Yan, M., Yu, P., 2015. An overview of densification, microstructure and mechanical property of additively manufactured Ti-6Al-4V: Comparison among selective laser melting, electron beam melting, laser metal deposition and selective laser sintering, and with conventional powder metallurgy, in: A. Lakshmanan (Ed.), Sintering Techniques of Materials, Intech.